ELSEVIER

International Journal of Solids and Structures 41 (2004) 4263–4277

INTERNATIONAL JOURNAL OF SOLIDS and STRUCTURES

www.elsevier.com/locate/ijsolstr

Stress concentrations near a fiber break in unidirectional composites with interfacial slip and matrix yielding

N. Ohno [a,*], S. Okabe [a], T. Okabe [b]

[a] *Department of Mechanical Engineering, Nagoya University, Chikusa-ku, Nagoya 464-8603, Japan*
[b] *Department of Aeronautics and Space Engineering, Tohoku University, Aoba-yama 01, Aoba-ku, Sendai 980-8579, Japan*

Received 19 March 2004; received in revised form 19 March 2004
Available online 30 April 2004

Abstract

In this study, 3D analytical solutions of stress profiles are obtained for the fibers adjacent to a broken fiber in unidirectional composites with interfacial slip and matrix yielding. To this end, a hexagonal fiber-array model containing a broken fiber is considered in order to derive differential equations based on a shear lag model. By assuming a bilinear stress profile for the broken fiber, and by introducing an elastoplastic shear modulus of the matrix, it is shown that all relevant material parameters are consolidated into a nondimensional characteristic length. The governing differential equations are then analytically solved under the condition that uniform axial deformation prevails in the second and third nearest-neighbor fibers, respectively. The resulting two analytical solutions are verified by numerically solving the governing equations more generally using a finite difference method. The analytical solutions are, moreover, compared with the detailed 3D finite element computations reported recently, leading to the validity of the present solutions and the effectiveness of the nondimensional characteristic length.

Keywords: Composite materials; Fiber break; Stress concentrations; Shear lag theory; Analytical solutions

1. Introduction

The longitudinal tensile failure of unidirectionally reinforced metal–matrix and polymer–matrix fiber composites is complex. Initially all fibers are supposed to be intact, although they are brittle. With the increase of tensile loads, fiber breaks can occur to cause stress concentrations in the adjacent fibers. The stress concentrations, then, may trigger the progressive failure of fibers, resulting in the final rupture of composites. The stress concentrations are affected by many factors such as the spacing of fibers, the

* Corresponding author. Tel.: +81-52-789-4475; fax: +81-52-789-5131.
E-mail address: ohno@mech.nagoya-u.ac.jp (N. Ohno).

0020-7683/$ - see front matter © 2004 Elsevier Ltd. All rights reserved.
doi:10.1016/j.ijsolstr.2004.03.018

characteristic of fiber/matrix interface, the yielding of matrix, the fiber to matrix ratio of elastic moduli, and so on. It is, therefore, important to evaluate the effects of these factors on the stress concentrations around fiber breaks in unidirectional fiber composites.

The shear lag concept introduced by Cox (1952) has been often employed to analyze the stress concentrations in unidirectional fiber composites. Such a study was first done by Hedgepeth (1961). He derived a 2D solution by applying the Fourier transformation to the governing equations of elastic lamina composites with the perfect bonding at fiber/matrix interface. His solution was extended to 3D elastic composites with square and hexagonal fiber arrays by Hedgepeth and Van Dyke (1967). While the 2D solution by Hedgepeth was shown to be in good agreement with continuum elasticity solutions (Beyerlein et al., 1996), the 3D solution by HVD was found to overestimate the stress concentrations of finite element analysis (Nedele and Wisnom, 1994a,b). Landis et al. (1999) improved the HVD model by formulating a shear lag model based on assumptions consistent with the principle of virtual work and the method of finite element analysis. Shear lag models have been also used to numerically simulate the progressive failure of fibers in unidirectional composites (Landis et al., 2000; Okabe et al., 2001, 2002; Ochiai et al., 2003; Goda, 2003).

The HVD model mentioned above is an excellent 3D solving method based on the Fourier transformation in the space of fiber displacements, though a double integral must be performed numerically. The HVD model, however, needs to be fairly sophisticated to take into account the slip at fiber/matrix interface around fiber breaks (Landis and McMeeking, 1999). For polymer–matrix and metal–matrix fiber composites, the slip at fiber/matrix interface usually occurs more significantly at higher applied loads. Matrix yielding also becomes significant with the increase in applied loads. It is, therefore, worthwhile to develop new analytical solutions which enable us to simply evaluate the stress concentrations around fiber breaks in the presence of interfacial slip and matrix yielding.

In the last decade, 2D and 3D finite element computations have been done in several studies to analyze the stress concentrations caused by a fiber break (Du and McMeeking, 1993; Nedele and Wisnom, 1994a,b; Goda, 1999; González and Llorca, 2001; Xia et al., 2001, 2002). Finite element computations in general allow us to correctly evaluate the stress concentrations, though they are numerical. Recently, both interfacial slip and matrix yielding were minutely taken into account in 3D detailed finite element computations by González and Llorca (2001) and Xia et al. (2001). Such detailed computations can be useful as references in developing new analytical solutions.

In this paper, by taking account of the slip at fiber/matrix interface as well as the yielding of matrix, 3D analytical solutions of stress profiles will be derived for the fibers adjacent to a broken fiber. For this purpose, a shear lag model will be built by supposing the hexagonally arrayed elastic fibers, with an initial break, embedded in the elastoplastic matrix with a secant shear modulus. The broken fiber will be assumed to have a bilinear profile of axial normal stress due to the interfacial slip, and the secant shear modulus of matrix will be represented by assuming the deformation theory of plasticity. Then, after showing that all material parameters in the basic equations are consolidated into a nondimensional characteristic length, analytical solutions will be obtained under the condition that uniform axial deformation prevails in the second and third nearest-neighbor fibers, respectively. The resulting two analytical solutions will be verified by numerically solving the governing equations more generally using a finite difference method, and by employing the results of the detailed 3D finite element analysis of González and Llorca (2001) and Xia et al. (2001).

2. Shear lag model

In this section, a shear lag model is developed to analyze the fiber stress profiles around a fiber break in a unidirectional composite subject to longitudinal tensile loading. We suppose that elastic fibers with a break

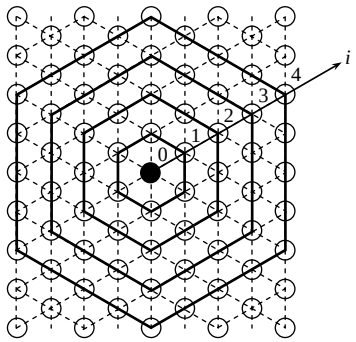

Fig. 1. Hexagonally arrayed fibers with a broken fiber labeled $i = 0$.

are hexagonally arrayed and embedded in an elastoplastic matrix, and that slip occurs at the fiber/matrix interface near the break.

Let the fibers be labeled $i = 0, 1, 2, \ldots$ so as to form concentric hexagons with the broken fiber located at the center (Fig. 1). Let us assume that all fibers belonging to the ith hexagon, i.e., the ith nearest-neighbor fibers, are identically deformed in the axial direction (Nedele and Wisnom, 1994a), and that the fibers, which have Young's modulus E_f, have an initial residual stress σ_{fr} in the axial direction. The shear lag concept then gives

$$\frac{du_i}{dz} = \frac{\sigma_i - \sigma_{fr}}{E_f}, \quad i = 0, 1, 2, \ldots, \tag{1}$$

where u_i and σ_i denote, respectively, the axial displacement and axial normal stress of the ith nearest-neighbor fibers, and z indicates the axial coordinate with its origin at the fiber break. We further assume that the fibers have a hexagonal cross section of side length a_f and area A_f, as shown in Fig. 2 (Suemasu, 1984). Fiber spacing s is then expressed in terms of fiber volume fraction f as follows:

$$s = \sqrt{3}\left(f^{-1/2} - 1\right)a_f. \tag{2}$$

Let us ignore the axial normal stress in matrix in conformity with the standard shear lag concept, though it was taken into account by Ochiai et al. (1991) and Landis and McMeeking (1999). This allows us to assume that the opposed surfaces of the ith and $i + 1$th nearest-neighbor fibers, which have been regarded as the hexagonal bars, have the same magnitude of shear stress, which will be denoted as $\tau_{i/i+1}$. The broken

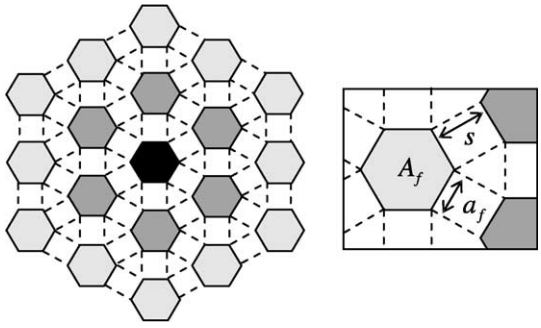

Fig. 2. Approximation of fibers by hexagonal bars of cross sectional area A_f and side length a_f.

fiber and the ith nearest-neighbor fibers then have the following equilibrium equations of forces, respectively:

$$A_{\mathrm{f}}\frac{\mathrm{d}\sigma_0}{\mathrm{d}z}+6a_{\mathrm{f}}\tau_{0/1}=0, \tag{3}$$

$$iA_{\mathrm{f}}\frac{\mathrm{d}\sigma_i}{\mathrm{d}z}-(2i-1)a_{\mathrm{f}}\tau_{i-1/i}+(2i+1)a_{\mathrm{f}}\tau_{i/i+1}=0, \quad i=1,2,3,\ldots \tag{4}$$

Here it is noted that the ith nearest-neighbor fibers consist of $6i$ fibers and have, in total, $6(2i-1)$ and $6(2i+1)$ faces on which $\tau_{i-1/i}$ and $\tau_{i/i+1}$ act, respectively.

When the shear stress acting on the broken fiber, $\tau_{0/1}$, reaches interfacial slip stress τ_{s} in the vicinity of the fiber break, the broken fiber has the axial stress profile $\sigma_0(z)$ illustrated in Fig. 3. Let us bilinearly approximate it, as shown by the dashed line in the figure. Then, $\sigma_0(z)$ and $\tau_{0/1}(z)$ have expressions

$$\sigma_0(z)=\begin{cases}\sigma_{\mathrm{f}}^{\infty}z/l, & 0\leqslant z\leqslant l,\\ \sigma_{\mathrm{f}}^{\infty}, & l\leqslant z,\end{cases} \tag{5}$$

$$\tau_{0/1}(z)=\begin{cases}-\tau_{\mathrm{s}}, & 0\leqslant z\leqslant l,\\ 0, & l\leqslant z,\end{cases} \tag{6}$$

where $\sigma_{\mathrm{f}}^{\infty}$ indicates the far field fiber stress related with applied strain ε^{∞},

$$\sigma_{\mathrm{f}}^{\infty}=E_{\mathrm{f}}\varepsilon^{\infty}+\sigma_{\mathrm{fr}}, \tag{7}$$

and l denotes the so-called stress recovery length. By use of Eqs. (3), (5) and (6), l is expressed as

$$l=\frac{A_{\mathrm{f}}\sigma_{\mathrm{f}}^{\infty}}{6a_{\mathrm{f}}\tau_{\mathrm{s}}}. \tag{8}$$

Matrix shear cannot be significant outside the first nearest-neighbor fibers, since $|\tau_{i/i+1}|\leqslant\tau_{\mathrm{s}}/(2i+1)$ according to Eqs. (4) and (6). For $\tau_{i/i+1}$ $(i=1,2,3,\ldots)$, therefore, we can assume the following equation based on the perfect bonding at fiber/matrix interface:

$$\tau_{i/i+1}=\frac{G_{\mathrm{m}}^{*}}{s}(u_{i+1}-u_i), \quad i=1,2,3,\ldots, \tag{9}$$

where G_{m}^{*} indicates an elastoplastic secant shear modulus of matrix. If the fiber break initially exists, the deformation in matrix cannot be extremely nonproportional even near the fiber break, so that the J_2 deformation theory is applicable to matrix plasticity. Then, on the assumption that applied strain ε^{∞} induces considerable plastic strain in the matrix, G_{m}^{*} can be represented as follows (see Appendix A):

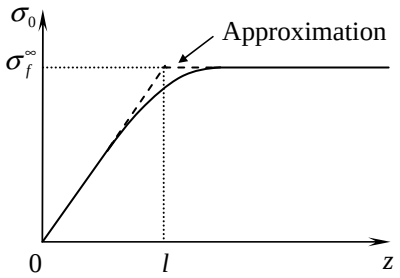

Fig. 3. Bilinear approximation of the stress profile of broken fiber.

$$G_{\mathrm{m}}^{*} \approx \left(\frac{1}{G_{\mathrm{m}}} + \frac{3\varepsilon_{\mathrm{mp}}^{\infty}}{\sigma_{\mathrm{m}}^{\infty}} \right)^{-1}, \tag{10}$$

where G_{m} indicates the elastic shear rigidity of matrix, and $\sigma_{\mathrm{m}}^{\infty}$ and $\varepsilon_{\mathrm{mp}}^{\infty}$ signify the far field axial stress and axial plastic strain in matrix, respectively.

Let us introduce nondimensional stresses

$$\Sigma_i = \frac{\sigma_i}{\sigma_{\mathrm{f}}^{\infty}}, \qquad T_{i/i+1} = \frac{\tau_{i/i+1}}{\sigma_{\mathrm{f}}^{\infty}}. \tag{11}$$

Then, eliminating $\tau_{i-1/i}$ and $\tau_{i/i+1}$ in Eq. (4) by use of Eqs. (3) and (9), differentiating the resulting equation with respect to z, and subsequently substituting Eq. (1), we have

$$\Sigma_1'' + 3\Sigma_2 - 3\Sigma_1 + \tfrac{1}{6}\Sigma_0'' = 0, \tag{12}$$

$$\Sigma_i'' + \frac{2i+1}{i}\Sigma_{i+1} - 4\Sigma_i + \frac{2i-1}{i}\Sigma_{i-1} = 0, \quad i = 2, 3, 4, \ldots \tag{13}$$

Here, $(\ )'$ indicates the differentiation with respect to a nondimensional axial coordinate

$$Z = \frac{z}{\Lambda}, \tag{14}$$

where

$$\Lambda = \left(\frac{E_{\mathrm{f}} A_{\mathrm{f}} s}{G_{\mathrm{m}}^{*} a_{\mathrm{f}}} \right)^{1/2}. \tag{15}$$

Eqs. (12) and (13), which we will solve analytically in Section 3, are the differential equations on fiber stresses rather than fiber displacements in contrast to the HVD model. Here it is noted that bilinear approximation (5) prescribes the following expression for Σ_0, which is regarded as a given input in solving Eqs. (12) and (13) for $\Sigma_i(Z)$, $i = 1, 2, 3, \ldots$:

$$\Sigma_0(Z) = \begin{cases} Z/L, & 0 \leqslant Z \leqslant L, \\ 1, & L \leqslant Z, \end{cases} \tag{16}$$

where L is the nondimensional stress recovery length, i.e.,

$$L = \frac{l}{\Lambda}. \tag{17}$$

Substituting Eqs. (8) and (15) into Eq. (17), and using Eq. (2) as well as $A_{\mathrm{f}}/a_{\mathrm{f}}^2 = 3\sqrt{3}/2$, we can show that

$$L = \left[\frac{G_{\mathrm{m}}^{*}}{24 E_{\mathrm{f}} (f^{-1/2} - 1)} \right]^{1/2} \frac{\sigma_{\mathrm{f}}^{\infty}}{\tau_{\mathrm{s}}}. \tag{18}$$

The boundary conditions to solve Eqs. (12) and (13) for Σ_i at $Z \geqslant 0$, $i = 1, 2, 3, \ldots$, can be written as

$$\lim_{Z \to \infty} \Sigma_i(Z) = 1, \quad i = 1, 2, 3, \ldots, \tag{19}$$

$$T_{i/i+1}(0) = 0, \quad i = 1, 2, 3, \ldots \tag{20}$$

Since Eq. (4) is rewritten as

$$T_{i/i+1} = -\frac{i}{2i+1} \frac{A_{\mathrm{f}}}{a_{\mathrm{f}} \Lambda} \Sigma_i' + \frac{2i-1}{2i+1} T_{i-1/i}, \quad i = 1, 2, 3, \ldots, \tag{21}$$

the second boundary condition, Eq. (20), is shown to take the following form by use of Eqs. (6), (8), $(11)_2$ and (17):

$$\Sigma_1'(0) = -\frac{1}{6L}, \quad \Sigma_i'(0) = 0, \quad i = 2, 3, 4, \ldots \tag{22}$$

Here it is noted that $\Sigma_1'(0) \neq 0$ because $\tau_{0/1}(0) \neq 0$ in shear lag modeling.

It is seen from Eqs. (12), (13), (19) and (22) that all related material parameters are consolidated into L; in other words, L represents the entire influence of material parameters in the shear lag model developed above. We, therefore, can call L the nondimensional characteristic length or, simply, the characteristic length.

3. Analytical solutions

If the Nth nearest-neighbor fibers constitute an outmost periphery subject to uniform axial deformation, we have $\Sigma_N = 1$. Now, applying this condition to the second and third nearest-neighbor fibers, respectively, we derive two analytical solutions, referred to as Solutions I and II.

3.1. Solution I

Let us suppose that the second nearest-neighbor fibers are subject to uniform axial deformation. Then, since

$$\Sigma_2 = 1, \tag{23}$$

Eq. (12) with $\Sigma_0(Z)$ approximated bilinearly as Eq. (16) is reduced to

$$\Sigma_1'' - 3\Sigma_1 + 3 = 0. \tag{24}$$

We notice that because of Eq. (16), not only Σ_0' but also Σ_1' has a discontinuity at $Z = L$. Hence, let $\Sigma_1^{\text{in}}(Z)$ and $\Sigma_1^{\text{out}}(Z)$ indicate $\Sigma_1(Z)$ in the intervals of $0 \leqslant Z \leqslant L$ and $L \leqslant Z$, respectively. Then, a general solution of Eq. (24) is written as

$$\Sigma_1^{\text{in}}(Z) = 1 + C_1 e^{\sqrt{3}Z} + C_2 e^{-\sqrt{3}Z}, \quad 0 \leqslant Z \leqslant L, \tag{25a}$$

$$\Sigma_1^{\text{out}}(Z) = 1 + C_3 e^{\sqrt{3}Z} + C_4 e^{-\sqrt{3}Z}, \quad L \leqslant Z, \tag{25b}$$

where C_1, C_2, C_3 and C_4 are integration constants. These constants can be determined using the boundary conditions (19) and $(22)_1$ as well as the continuity conditions of Σ_1 and $T_{1/2}$ at $Z = L$,

$$\Sigma_1^{\text{out}}(\infty) = 1, \quad \Sigma_1^{\text{in}'}(0) = -\frac{1}{6L}, \quad \Sigma_1^{\text{in}}(L) = \Sigma_1^{\text{out}}(L), \quad T_{1/2}^{\text{in}}(L) = T_{1/2}^{\text{out}}(L). \tag{26}$$

By using Eq. (21) along with Eqs. (6), (8), $(11)_2$ and (17), the last condition above is rewritten as

$$\Sigma_1^{\text{in}'}(L) + \frac{1}{6L} = \Sigma_1^{\text{out}'}(L). \tag{27}$$

The constants are thus determined as

$$C_1 = \frac{-e^{-\sqrt{3}L}}{12\sqrt{3}L}, \quad C_2 = \frac{2 - e^{-\sqrt{3}L}}{12\sqrt{3}L}, \quad C_3 = 0, \quad C_4 = \frac{2 - e^{\sqrt{3}L} - e^{-\sqrt{3}L}}{12\sqrt{3}L}. \tag{28}$$

Consequently, Solution I provides the stress concentration factor, SCF, and the positively affected length, PAL, of the first nearest-neighbor fibers with analytical evaluations:

$$\mathrm{SCF} = \frac{1 - \mathrm{e}^{-\sqrt{3}L}}{6\sqrt{3}L}, \tag{29}$$

$$\frac{\mathrm{PAL}}{\Lambda} = \frac{\ln(2\mathrm{e}^{\sqrt{3}L} - 1)}{2\sqrt{3}}. \tag{30}$$

It is seen from Eq. (29) that the SCF takes the maximum and minimum values of 1/6 and 0, as $L \to 0$ and $L \to \infty$, respectively. Thus, we can say that the SCF is higher, when the nondimensional stress recovery length L is shorter.

3.2. Solution II

If the third nearest-neighbor fibers are supposed to be subject to uniform axial deformation,

$$\Sigma_3 = 1. \tag{31}$$

Eqs. (12) and (13), into which Eq. (16) is substituted, are then reduced to

$$\Sigma_1'' + 3\Sigma_2 - 3\Sigma_1 = 0, \tag{32}$$

$$\Sigma_2'' - 4\Sigma_2 + \tfrac{3}{2}\Sigma_1 + \tfrac{5}{2} = 0. \tag{33}$$

Eqs. (32) and (33) are the simultaneous equations to determine $\Sigma_1(Z)$ and $\Sigma_2(Z)$. It is seen that they have a particular solution

$$\Sigma_1(Z) = \Sigma_2(Z) = 1 \tag{34}$$

and homogeneous equations

$$\Sigma_1'' - 3\Sigma_1 + 3\Sigma_2 = 0, \tag{35}$$

$$\tfrac{3}{2}\Sigma_1 + \Sigma_2'' - 4\Sigma_2 = 0. \tag{36}$$

Eqs. (32) and (33), therefore, have the following general solution, in which the interval is divided into $0 \leqslant Z \leqslant L$ and $L \leqslant Z$ as in Solution I:

$$\Sigma_1^{\mathrm{in}}(Z) = 1 + \sum_{n=1}^{4} D_n \mathrm{e}^{\lambda_n Z}, \quad 0 \leqslant Z \leqslant L, \tag{37a}$$

$$\Sigma_1^{\mathrm{out}}(Z) = 1 + \sum_{n=1}^{4} D_{4+n} \mathrm{e}^{\lambda_n Z}, \quad L \leqslant Z, \tag{37b}$$

$$\Sigma_2^{\mathrm{in}}(Z) = 1 + \sum_{n=1}^{4} D_n \kappa_n \mathrm{e}^{\lambda_n Z}, \quad 0 \leqslant Z \leqslant L, \tag{38a}$$

$$\Sigma_2^{\mathrm{out}}(Z) = 1 + \sum_{n=1}^{4} D_{4+n} \kappa_n \mathrm{e}^{\lambda_n Z}, \quad L \leqslant Z, \tag{38b}$$

where $D_1, D_2, \ldots$ and D_8 are integration constants, and λ_n and κ_n $(n = 1, 2, 3, 4)$ are obtained from the characteristic equation of Eqs. (35) and (36) as follows:

$$\left.\begin{matrix}\lambda_1\\ \lambda_2\end{matrix}\right\} = \pm\left(\frac{7-\sqrt{19}}{2}\right)^{1/2}, \quad \left.\begin{matrix}\lambda_3\\ \lambda_4\end{matrix}\right\} = \pm\left(\frac{7+\sqrt{19}}{2}\right)^{1/2}, \tag{39}$$

$$\kappa_n = \frac{3-\lambda_n^2}{3}, \quad n = 1, 2, 3, 4. \tag{40}$$

The constants $D_1, D_2, \ldots$ and D_8 can be determined using the boundary conditions (19) and (22) as well as the continuity conditions of Σ_i and $T_{i/i+1}$, $i = 1, 2$, at $Z = L$,

$$\begin{aligned}&\Sigma_1^{\text{out}}(\infty) = 1, \quad \Sigma_2^{\text{out}}(\infty) = 1, \quad \Sigma_1^{\text{in}'}(0) = -\frac{1}{6L}, \quad \Sigma_2^{\text{in}'}(0) = 0,\\ &\Sigma_1^{\text{in}}(L) = \Sigma_1^{\text{out}}(L), \quad \Sigma_2^{\text{in}}(L) = \Sigma_2^{\text{out}}(L), \quad T_{1/2}^{\text{in}}(L) = T_{1/2}^{\text{out}}(L), \quad T_{2/3}^{\text{in}}(L) = T_{2/3}^{\text{out}}(L),\end{aligned} \tag{41}$$

where the last two conditions become Eq. (27) and $\Sigma_2^{\text{in}'}(L) = \Sigma_2^{\text{out}'}(L)$, respectively, because of Eq. (21). Then, applying the above conditions to Eqs. (37a)–(38b), we have a system of equations by which $D_1, D_2, \ldots$ and D_8 are determined, with the help of a manipulation software Mathematica, as follows:

$$\begin{aligned}&D_1 = \frac{\kappa_3 \mathrm{e}^{-\lambda_1 L}}{12(\kappa_1-\kappa_3)\lambda_1 L}, \qquad D_2 = \frac{-\kappa_3(2-\mathrm{e}^{-\lambda_1 L})}{12(\kappa_1-\kappa_3)\lambda_1 L},\\ &D_3 = \frac{-\kappa_1 \mathrm{e}^{-\lambda_3 L}}{12(\kappa_1-\kappa_3)\lambda_3 L}, \qquad D_4 = \frac{\kappa_1(2-\mathrm{e}^{-\lambda_3 L})}{12(\kappa_1-\kappa_3)\lambda_3 L},\\ &D_5 = 0, \qquad D_6 = \frac{-\kappa_3(2-\mathrm{e}^{\lambda_1 L}-\mathrm{e}^{-\lambda_1 L})}{12(\kappa_1-\kappa_3)\lambda_1 L},\\ &D_7 = 0, \qquad D_8 = \frac{\kappa_1(2-\mathrm{e}^{\lambda_3 L}-\mathrm{e}^{-\lambda_3 L})}{12(\kappa_1-\kappa_3)\lambda_3 L}.\end{aligned} \tag{42}$$

According to Solution II, therefore, the first nearest-neighbor fibers have

$$\mathrm{SCF} = \frac{\kappa_1\lambda_1(1-\mathrm{e}^{-\lambda_3 L}) - \kappa_3\lambda_3(1-\mathrm{e}^{-\lambda_1 L})}{6(\kappa_1-\kappa_3)\lambda_1\lambda_3 L}. \tag{43}$$

This SCF also takes the maximum and minimum values of 1/6 and 0, as $L \to 0$ and $L \to \infty$ respectively. The PAL by Solution II is evaluated by numerically solving $\Sigma_1^{\text{in}}(Z) = 1$.

4. Discussion

Solutions I and II have been obtained by analytically solving Eqs. (12) and (13) under the condition that uniform axial deformation prevails in the second and third nearest-neighbor fibers, respectively. In this section, first, the validity of this condition is discussed by numerically solving Eqs. (12) and (13) more generally; subsequently, Solutions I and II are compared with the detailed 3D finite element computations done by González and Llorca (2001) and Xia et al. (2001).

4.1. Comparison with finite difference analysis

Discretizing Eqs. (12) and (13) by use of a finite difference method, we have numerically analyzed the fiber stress profiles more generally than in Solutions I and II (see Appendix B). The distribution of SCFs

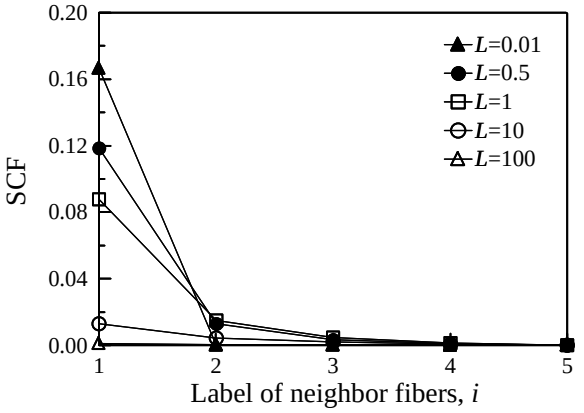

Fig. 4. SCF of ith nearest-neighbor fibers by finite difference analysis with $\Sigma_5 = 1$.

shown in Fig. 4 has been thus obtained on the assumption that uniform axial deformation prevails in the fifth nearest-neighbor fibers. The nondimensional characteristic length L, which represents the entire influence of material parameters, has been changed in this finite difference analysis, so that in the figure, the SCF of the first nearest-neighbor fibers ranges from zero, the minimum, to 1/6, the maximum. It is seen from Fig. 4 that the fourth nearest-neighbor fibers always have almost zero SCFs, and that the second and third nearest-neighbor fibers have SCFs less than 0.015 and 0.005, respectively. This shows the validity of the assumption used in Solution II that the third nearest-neighbor fibers are subject to uniform axial deformation.

Fig. 5(a) and (b) compare the two analytical solutions and the finite difference analysis mentioned above with respect to the SCF and PAL of the first nearest-neighbor fibers. As seen from the figures, Solutions I and II give nearly the same SCFs and PALs as the finite difference analysis; especially, the SCF and PAL by Solution II are very close to those by the finite difference analysis. Verification is, thus, made for Solutions I and II so that they can be useful analytical solutions based on the shear lag model described in Section 2.

4.2. Comparison with finite element analysis

González and Llorca (2001) performed 3D finite element analysis to analyze the stress profiles of the fibers adjacent to a broken fiber in a unidirectional composite Ti–6Al–4V/SiC. In their analysis, elastic fibers were hexagonally arrayed in an elastic–perfectly plastic matrix, and Coulomb's friction law was assumed to allow the interfacial slip near the fiber break. Let us discuss Solutions I and II in the light of their finite element analysis. The material parameters necessary for applying Solutions I and II to their finite element analysis have been taken from their paper (Table 1). We thus have $L = 2.5$ using Eqs. (10) and (18) with $\varepsilon_{\mathrm{mp}}^{\infty} = \varepsilon^{\infty} - (\sigma_{\mathrm{m}}^{\infty} - \sigma_{\mathrm{mr}})/E_{\mathrm{m}}$. The axial profiles of σ_1 by Solutions I and II with $L = 2.5$ are compared with that of the finite element analysis in Fig. 6, where R denotes the radius of fibers. It is seen from the figure that Solutions II has good agreement with the finite element analysis in the positively affected interval, $0 \leqslant z \leqslant \mathrm{PAL}$, while Solution I gives lower stress in this interval. Thus, the 3D finite element analysis verifies Solution II.

Solutions I and II have singular points at $z/R = 16.5$ (Fig. 6), which are due to the bilinear approximation of $\sigma_0(z)$ shown in Fig. 7. In order to examine the influence of the bilinear approximation, the axial profile of σ_0 determined by the finite element analysis has been input into Eqs. (12) and (13) for performing another finite difference computation. This computation, for which we have assumed $\Sigma_3 = 1$ as in Solution

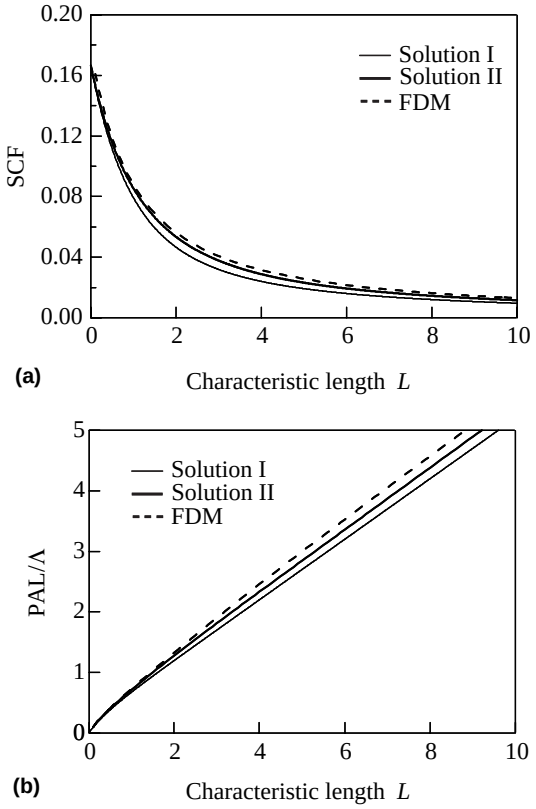

Fig. 5. Comparison of analytical solutions and finite difference analysis with $\Sigma_5 = 1$; (a) SCF and (b) PAL of first nearest-neighbor fibers.

Table 1
Data for comparison with finite element analysis of González and Llorca (2001) and Xia et al. (2001)

	González–Llorca	Xia et al.
Applied strain, ε^{∞} (%)	1.00	0.94
Fiber volume fraction, f	0.35	0.4
Young's modulus of fibers, E_{f} (GPa)	330	400
Young's modulus of matrix, E_{m} (GPa)	110	115
Poisson's ratio of matrix, ν_{m}	0.33	0.3
Residual stress of fibers, σ_{fr} (MPa)	−876	−540
Residual stress of matrix, σ_{mr} (MPa)	471	360
Interfacial slip stress, τ_{s} (MPa)	70	58 ($\mu = 0.25$)
		120 ($\mu = 0.5$)
		193 ($\mu = 0.9$)
Far field fiber stress, $\sigma_{\mathrm{f}}^{\infty}$ (MPa)	2420	3200
Far field matrix stress, $\sigma_{\mathrm{m}}^{\infty}$ (MPa)	1130	1000

II, has resulted in the profile of σ_1 depicted by a chain line in Fig. 6. The bilinear approximation is seen to exert little influence on the profile of σ_1 in the interval of $0 \leqslant z \leqslant \mathrm{PAL}$.

Now, we use the results of 3D finite element analysis reported by Xia et al. (2001). They assumed three values of Coulomb's friction coefficient μ in order to study in detail the effect of interfacial slip near a fiber

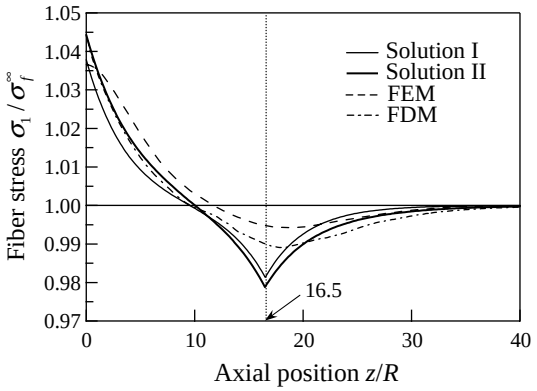

Fig. 6. Stress profiles of first nearest-neighbor fibers by analytical solutions, finite element analysis (González and Llorca, 2001), and finite difference analysis with $\Sigma_3 = 1$ and $\sigma_0(z)$ determined by finite element analysis.

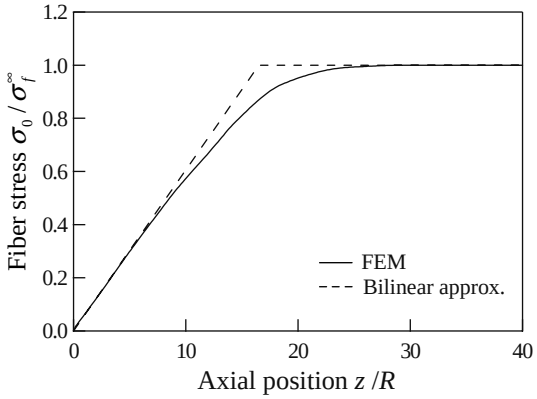

Fig. 7. Stress profile of broken fiber by finite element analysis (González and Llorca, 2001), and its bilinear approximation.

break in a unidirectional composite IMI-834 Ti/SCS-6 SiC, which was modeled by hexagonally arrayed elastic fibers and an elastoplastic matrix with strain hardening. For their analysis, L is evaluated to be $L = 4.0$, 1.9 and 1.2 in the three cases of $\mu = 0.25$, 0.5 and 0.9, respectively, by use of the data given in Table 1. The SCFs and PALs determined by Xia et al. are plotted as a function of L in Fig. 8(a) and (b), respectively, to compare their computations with Solutions I and II. The results of González and Llorca are also plotted in the figures. It is seen that Solutions I and II have fairly good agreement with the 3D finite element computations. We, therefore, can say that Solutions I and II are effective for estimating the SCF and PAL of the first nearest-neighbor fibers.

Let us discuss the effects of interfacial slip and matrix yielding by means of the nondimensional characteristic length L. Since L is inversely proportional to τ_s in Eq. (18), L ranges widely in the three cases of $\mu = 0.25$, 0.5 and 0.9, as seen in Fig. 8. Consequently, interfacial slip significantly influences the SCFs near a fiber break. The effect of matrix yielding can be examined by disregarding $\varepsilon_{pm}^{\infty}$ in evaluating L. If $\varepsilon_{pm}^{\infty}$ is ignored, G_m^* becomes equal to G_m, as seen from Eq. (10). Then, since $L \propto \sqrt{G_m^*}$ in Eq. (18), and since $G_m > G_m^*$, L is overestimated, resulting in underestimating the SCFs. Thus, the nondimensional characteristic length L, which is represented as Eq. (18), is useful for discussing the effects of interfacial slip and matrix yielding.

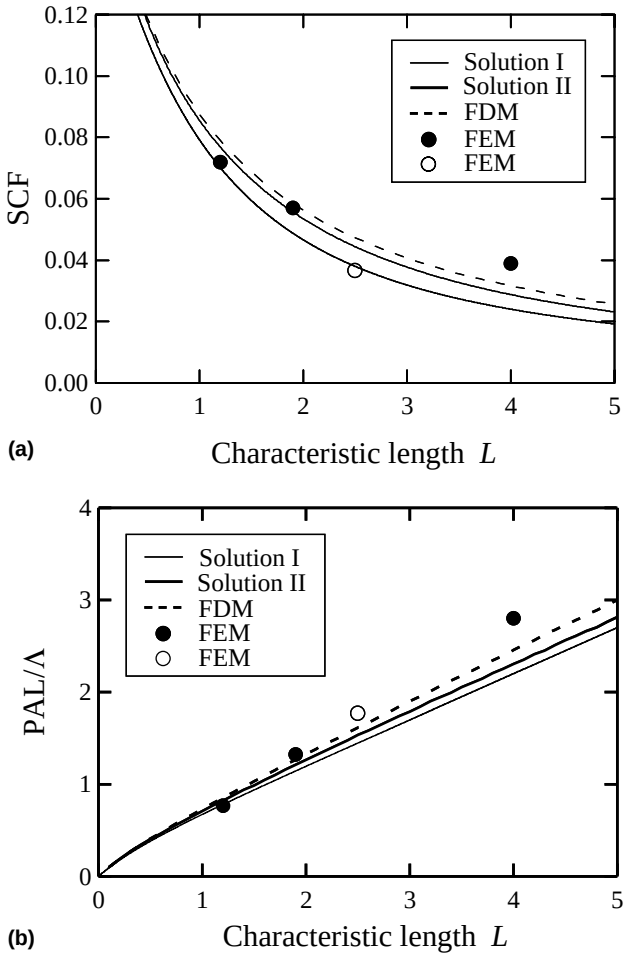

Fig. 8. Comparison of analytical solutions, finite difference analysis with $\Sigma_5 = 1$, and finite element analysis (● Xia et al., 2001; ○ González and Llorca, 2001); (a) SCF and (b) PAL of first nearest-neighbor fibers.

A fiber break was engendered not before but after applying tensile strain ε^{∞} in the finite element analysis of González and Llorca (2001). Such a fiber break causes matrix shear to follow tensile strain, so that nonproportional deformation occurs in the matrix around the break. This matrix shear can be nearly elastic, since the development of matrix shear stress is limited by interfacial slip stress τ_s, and since τ_s is usually much smaller than the yield stress of matrix. Nearly elastic behavior in the shear following tensile strain was observed in combined tension–torsion experiments, for example, by Ohashi et al. (1981). For the fiber break introduced after applying tensile strain, therefore, it may be appropriate to assume Eq. (9) with G_m^* replaced by G_m, leading to

$$L = \left[\frac{G_m}{24E_f(f^{-1/2}-1)}\right]^{1/2}\frac{\sigma_f^{\infty}}{\tau_s}. \tag{44}$$

Their finite element analysis then has $L = 3.0$ instead of $L = 2.5$. This change in L, however, induces only a little decrease in the SCF (see Fig. 8), so that the profiles of σ_1 by Solutions I and II in Fig. 6 remain valid.

Incidentally, the discussion above suggests that the SCF near a fiber break induced after tensile loading is likely to be lower than that near an initially existing fiber break. This tendency was found to be noticeable in the 3D detailed finite element analysis of an aluminum–matrix composite with the perfect bonding at fiber/matrix interface (Xia et al., 2002).

5. Concluding remarks

This study was concerned with 3D analytical evaluations of the stress concentrations near a fiber break in unidirectional composites with interfacial slip and matrix yielding. First, a shear lag model was developed by considering hexagonally arrayed elastic fibers with an initial break in an elastoplastic matrix. The broken fiber was assumed to have a bilinear stress profile due to interfacial slip, and the matrix to have a secant shear modulus to take matrix yielding into account. It was, thus, shown that all relevant material parameters are consolidated into a nondimensional characteristic length. Then, the governing differential equations were analytically solved under the condition that uniform axial deformation prevails in the second and third nearest-neighbor fibers, respectively. The resulting two analytical solutions, Solutions I and II, were examined by numerically solving the differential equations more generally as well as by using the results of detailed 3D finite element analysis reported recently. It was thus found that especially Solution II has good agreement with these numerical results, and that the nondimensional characteristic length is effective for evaluating the stress concentrations affected by interfacial slip and matrix yielding.

Let us emphasize the following: In this study, we dealt with the differential equations on fiber stresses rather than fiber displacements in contrast to the HVD model. In the presence of interfacial sliding, then, the bilinearly approximated stress profile of the broken fiber functioned as a given input to determining the stress profiles of adjacent fibers. We thus derived Solutions I and II as well as the nondimensional characteristic length. It will be subjects in our future studies to apply Solutions I and II to estimating the stress concentrations near multiple fiber breaks and to predicting the tensile strength of composites.

The radial variation of matrix shear stress around a fiber break, which was not considered in this study, is not negligible if fiber volume fraction is considerably small (Clyne and Withers, 1993; Xia et al., 2002). It will be also a subject in our future studies to extend Solutions I and II by taking account of the radial variation of matrix shear stress.

Acknowledgements

The authors are grateful to Dr. S. Biwa, Nagoya University, for his suggestion regarding the analytical solutions in Section 3. Gratitude is also expressed to Dr. K. Goda, Yamaguchi University, for his helpful comments on the results in the present study.

Appendix A. Elastoplastic secant shear modulus of matrix

The J_2 deformation theory allows matrix tensile and shear strains, ε_m and γ_m, to be related with matrix tensile and shear stresses, σ_m and τ_m, as follows:

$$\varepsilon_m = \left(\frac{1}{E_m} + \frac{\bar{\varepsilon}_{mp}}{\bar{\sigma}_m}\right)\sigma_m, \qquad \gamma_m = \left(\frac{1}{G_m} + \frac{3\bar{\varepsilon}_{mp}}{\bar{\sigma}_m}\right)\tau_m, \tag{A.1}$$

where E_m and G_m indicates the tensile and shear rigidities of matrix, and $\bar{\sigma}_m$ and $\bar{\varepsilon}_{mp}$ denote equivalent matrix stress and equivalent matrix plastic strain, respectively. Since $\gamma_m \approx (u_{i+1} - u_i)/s$, Eq. $(A.1)_2$ provides the secant modulus in Eq. (9), G_m^*, with an expression

$$G_{\mathrm{m}}^{*} \approx \left(\frac{1}{G_{\mathrm{m}}} + \frac{3\bar{\varepsilon}_{\mathrm{mp}}}{\bar{\sigma}_{\mathrm{m}}} \right)^{-1}. \tag{A.2}$$

Let us remember that matrix shear cannot be significant outside the first nearest-neighbor fibers, and that G_{m}^{*} applies to such shear. Then, on the assumption that applied loads induce considerable axial stress and axial plastic strain in the matrix, we may have $\bar{\sigma}_{\mathrm{m}} = (\sigma_{\mathrm{m}}^2 + 3\tau_{\mathrm{m}}^2)^{1/2} \approx \sigma_{\mathrm{m}}^{\infty}$ and $\bar{\varepsilon}_{\mathrm{mp}} = (\varepsilon_{\mathrm{mp}}^2 + \gamma_{\mathrm{mp}}^2/3)^{1/2} \approx \varepsilon_{\mathrm{mp}}^{\infty}$ outside the first nearest-neighbor fibers, so that G_{m}^{*} becomes

$$G_{\mathrm{m}}^{*} \approx \left(\frac{1}{G_{\mathrm{m}}} + \frac{3\varepsilon_{\mathrm{mp}}^{\infty}}{\sigma_{\mathrm{m}}^{\infty}} \right)^{-1}, \tag{A.3}$$

where $\sigma_{\mathrm{m}}^{\infty}$ and $\varepsilon_{\mathrm{mp}}^{\infty}$ signify the axial normal stress and axial plastic strain in the far field matrix, respectively.

Appendix B. Finite difference method

In order to solve Eqs. (12) and (13) more generally than Solutions I and II, we employed the central finite difference approximation of Σ_i'',

$$\Sigma_{i,k}'' \approx \frac{\Sigma_{i,k-1} - 2\Sigma_{i,k} + \Sigma_{i,k+1}}{(\Delta Z)^2}, \quad k = 0, 1, 2, \ldots, K_{\infty} - 1, \tag{B.1}$$

where $\Sigma_{i,k}$ $(k = -1, 0, 1, \ldots, K_L, \ldots, K_{\infty})$ indicates the value of Σ_i at the kth point in the interval $0 \leqslant Z \leqslant Z_{\infty}$ divided equally into K_{∞} segments with a length of $\Delta Z = Z_{\infty}/K_{\infty}$. Here, it is noted that a fictitious point, $k = -1$, was introduced for convenience so as to represent the symmetry of $\Sigma_i(Z)$ with respect to $Z = 0$. It is also noted that the stress recovery point in the broken fiber, $Z = L$, was labeled $k = K_L$, where $K_L = L/\Delta Z$.

The uniform axial deformation in the Nth nearest-neighbor fibers was assumed, so that

$$\Sigma_{N,k} = 1, \quad k = -1, 0, 1, \ldots, K_{\infty}. \tag{B.2}$$

Moreover, the symmetry of $\Sigma_i(Z)$ with respect to $Z = 0$ and the vanishing stress concentration at $Z = Z_{\infty}$ were used as the boundary conditions. Then,

$$\Sigma_{i,-1} = \Sigma_{i,1}, \quad i = 0, 1, \ldots, N, \tag{B.3}$$

$$\Sigma_{i,K_{\infty}} = 1, \quad i = 0, 1, \ldots, N. \tag{B.4}$$

Thus, Eqs. (12) and (13) with $\Sigma_0(Z)$ approximated bilinearly as Eq. (16) were reduced to the simultaneous linear equations to determine $\Sigma_{i,k}$ $(i = 1, 2, \ldots, N-1;\ k = 0, 1, \ldots, K_{\infty} - 1)$. Incidentally, the bilinear approximation of $\Sigma_0(Z)$ rendered Σ_0'' in Eq. (12) nonzero at $Z = 0$ and $Z = Z_L$; the value of Σ_0'' at $Z = 0$ was evaluated to be $\Sigma_{0,0}''(0) = 2/[K_L(\Delta Z)^2]$ by use of Eqs. (16), (B.1) and (B.3), while $\Sigma_{0,K_L}''(L) = -1/[K_L(\Delta Z)^2]$ by substituting Eq. (16) into Eq. (B.1).

References

Beyerlein, I.J., Phoenix, S.L., Sastry, A.M., 1996. Comparison of shear-lag theory and continuum fracture mechanics for modeling fiber and matrix stresses in an elastic cracked composite lamina. Int. J. Solids Struct. 33, 2543–2574.

Clyne, T.W., Withers, P.J., 1993. An Introduction to Metal Matrix Composites. Cambridge University Press, Cambridge. pp. 20–24.

Cox, H.L., 1952. The elasticity and strength of paper and other fibrous materials. Br. J. Appl. Phys. 3, 72–79.

Du, Z.-Z., McMeeking, R.M., 1993. Control of strength anisotropy of metal matrix fiber composites. J. Comput.-Aided Mater. Des. 1, 243–264.

Goda, K., 1999. The role of interfacial debonding in increasing the strength and reliability of unidirectional fibrous composites. Compos. Sci. Technol. 59, 1871–1879.

Goda, K., 2003. A strength reliability model by Markov process of unidirectional composites with fibers placed in hexagonal arrays. Int. J. Solids Struct. 40, 6813–6837.

González, C., Llorca, J., 2001. Micromechanical modelling of deformation and failure in Ti–6Al–4V/SiC composites. Acta Mater. 49, 3505–3519.

Hedgepeth, J.M., 1961. Stress concentrations in filamentary structures. NASA Tech. Note D-882.

Hedgepeth, J.M., Van Dyke, P., 1967. Local stress concentrations in imperfect filamentary composite materials. J. Compos. Mater. 1, 294–309.

Landis, C.M., McMeeking, R.M., 1999. Stress concentrations in composites with interface sliding, matrix stiffness and uneven fiber spacing using shear lag theory. Int. J. Solids Struct. 36, 4333–4361.

Landis, C.M., McGlockton, M.A., McMeeking, R.M., 1999. An improved shear lag model for broken fibers in composite materials. J. Compos. Mater. 33, 667–680.

Landis, C.M., Beyerlein, I.J., McMeeking, R.M., 2000. Micromechanical simulation of the failure of fiber reinforced composites. J. Mech. Phys. Solids 48, 621–648.

Nedele, M.R., Wisnom, M.R., 1994a. Stress concentration factors around a broken fibre in a unidirectional carbon fibre-reinforced epoxy. Composites 25, 549–557.

Nedele, M.R., Wisnom, M.R., 1994b. Three-dimensional finite element analysis of the stress concentration at a single fibre break. Compos. Sci. Technol. 51, 517–524.

Ochiai, S., Schulte, K., Peters, P.W.M., 1991. Strain concentration factors for fibers and matrix in unidirectional composites. Compos. Sci. Technol. 41, 237–256.

Ochiai, S., Tanaka, H., Kimura, S., Tanaka, M., Hojo, M., Okuda, K., 2003. Modeling of residual stress-induced stress–strain behavior of unidirectional brittle fiber/brittle matrix composite with weak interface. Compos. Sci. Technol. 63, 1027–1040.

Ohashi, Y., Kurita, Y., Suzuki, T., Tokuda, M., 1981. Effect of curvature of the strain trajectory on the plastic behavior of brass. J. Mech. Phys. Solids 29, 69–86.

Okabe, T., Takeda, N., 2002. Elastoplastic shear-lag analysis of single-fiber composites and strength prediction of unidirectional multi-fiber composites. Composites, Part A 33, 1327–1335.

Okabe, T., Takeda, N., Kamoshida, Y., Shimizu, M., Curtin, W.A., 2001. A 3D shear-lag model considering micro-damage and statistical strength prediction of unidirectional fiber-reinforced composites. Compos. Sci. Technol. 61, 1773–1787.

Suemasu, H., 1984. Probabilistic aspects of strength of unidirectional fibre-reinforced composites with matrix failure. J. Mater. Sci. 19, 574–584.

Xia, Z., Curtin, W.A., Peters, P.W.M., 2001. Multiscale modeling of failure in metal matrix composites. Acta Mater. 49, 273–287.

Xia, Z., Okabe, T., Curtin, W.A., 2002. Shear-lag versus finite element models for stress transfer in fiber-reinforced composites. Compos. Sci. Technol. 62, 1141–1149.